ACS APPLIED MATERIALS & INTERFACES

Research Article

www.acsami.org

Ultrasensitive Hydrogen Sensor Based on Pd^0-Loaded SnO_2 Electrospun Nanofibers at Room Temperature

Zhaojie Wang,[†] Zhenyu Li,*[,†,‡] Tingting Jiang,[†] Xiuru Xu,[†] and Ce Wang*[,†]

[†]Alan G. MacDiarmid Institute, Jilin University, Changchun 130012, P. R. China.

[‡]Australian Future Fibres Research & Innovation Centre, Institute for Frontier Materials, Deakin University, Geelong, Victoria 3217, Australia.

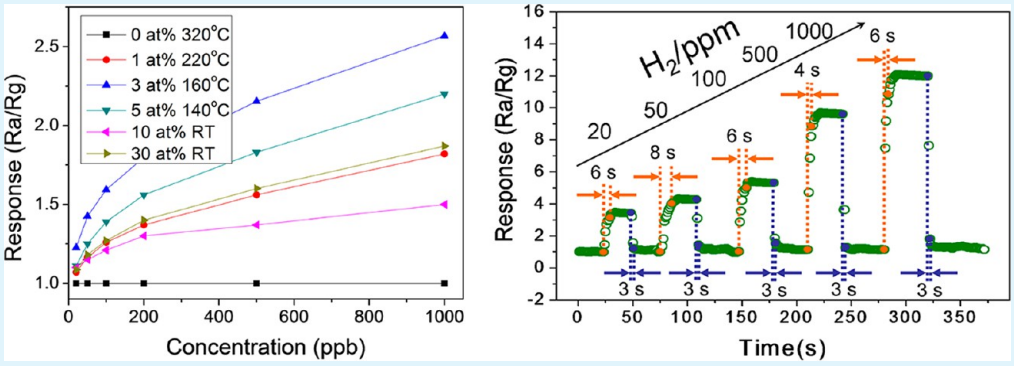

ABSTRACT: Pd^0-loaded SnO_2 nanofibers have been successfully synthesized with different loaded levels via electrospinning process, sintering technology, and in situ reduction. This simple strategy could be expected to extend for the fabrication of similar metal−oxide loaded nanofibers using different precursors. The morphological and structural characteristics of the resultant product were investigated by scanning electron microscopy (SEM), transmission electron microscopy (TEM), X-ray diffraction (XRD), and X-ray photoelectron spectra (XPS). To demonstrate the usage of such Pd^0-loaded SnO_2 nanomaterial, a chemical gas sensor has been fabricated and investigated for H_2 detection. The sensing performances versus Pd^0-loaded levels have been investigated in detail. An ultralow limit of detection (20 ppb), high response, fast response and recovery, and selectivity have been obtained on the basis of the sensors operating at room temperature. The combination of SnO_2 crystal structure and catalytic activity of Pd^0-loaded gives a very attractive sensing behavior for applications as real-time monitoring gas sensors.

KEYWORDS: *hydrogen sensors, Pd^0-loaded, SnO_2 nanofibers, room temperature, crystal structure, catalytic activity*

1. INTRODUCTION

Hydrogen (H_2) as a clean and sustainable energy carrier is being widely used in energy generation.[1,2] Simultaneously, it is facile to explosive under a concentration range (4−75%) and low ignition energy (0.02 mJ).[3] Thereby, a reliable hydrogen sensor is needed to detect a leakage from the storage and transportation. Like other semiconductor type gas sensors, SnO_2, which has been mostly conducted on H_2 sensor, remains a future challenge for the development of low operating temperature, limit of detection, high sensitivity, fast response and recovery, and high selectivity.[4−10]

As we know, the working mechanism of SnO_2-based H_2 sensors lies in the convection of electrical conductivity due to surface reactions such as reduction caused by H_2 exposures.[11,12] Because these surface reactions depend on the active centers and the defects existing on the surface layer of materials, the sensor response is usually determined by the surface-to-volume ratio of materials. To satisfy this requirement, researchers have developed one-dimensional electrospun nanofibers as highly sensitive H_2 sensors because of the ultrahigh surface-to-volume ratio, implying those large surface activities, reactions at grain boundaries and the congruence of the carrier screening length with their lateral dimensions. Therefore, promising results of the H_2 sensing performance of SnO_2-based nanofibers have been reported in our previous research.[13−16]

In practice, the optimized operating temperature of these sensors are still very high, which brings about much inconvenience for practical applications and sometimes is even unsafe for detecting combustion gases. One of the most effective methods is functionalizing the material with catalytically active metals. Because of its electrical resistivity changes when palladium absorb hydrogen to form a hydride (PdH_x), Pd-functionalized nanostructures have developed as a novel candidate in decrease operating temperature toward oxygen and hydrogen.[17,18] For example, Lee et al. have reported that Pd-doped SnO_2 nanorod thin film sensor exhibited 6 time

Received: November 26, 2012
Accepted: February 27, 2013
Published: February 27, 2013

   dx.doi.org/10.1021/am3028553 | ACS Appl. Mater. Interfaces 2013, 5, 2013−2021

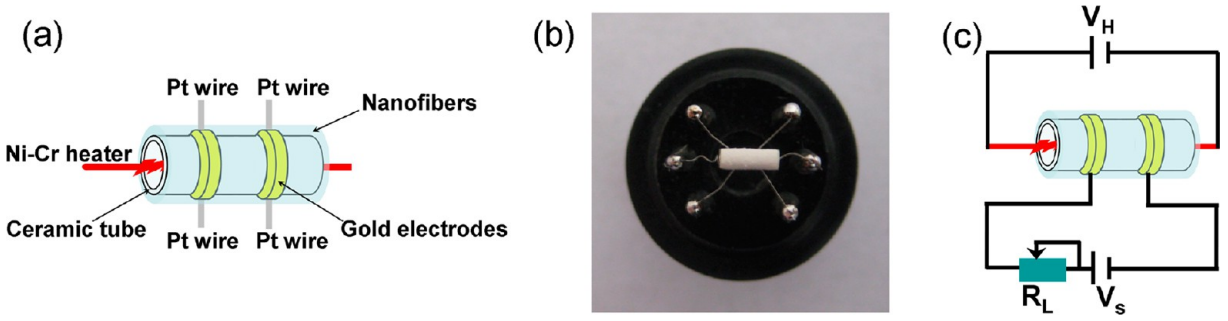

Figure 1. (a) Schematic image of the nanofibers sensor, (b) photograph of the SnO_2 nanofiber sensor, and (c) schematic diagram of the electrical circuit for measuring the nanofiber gas sensor.

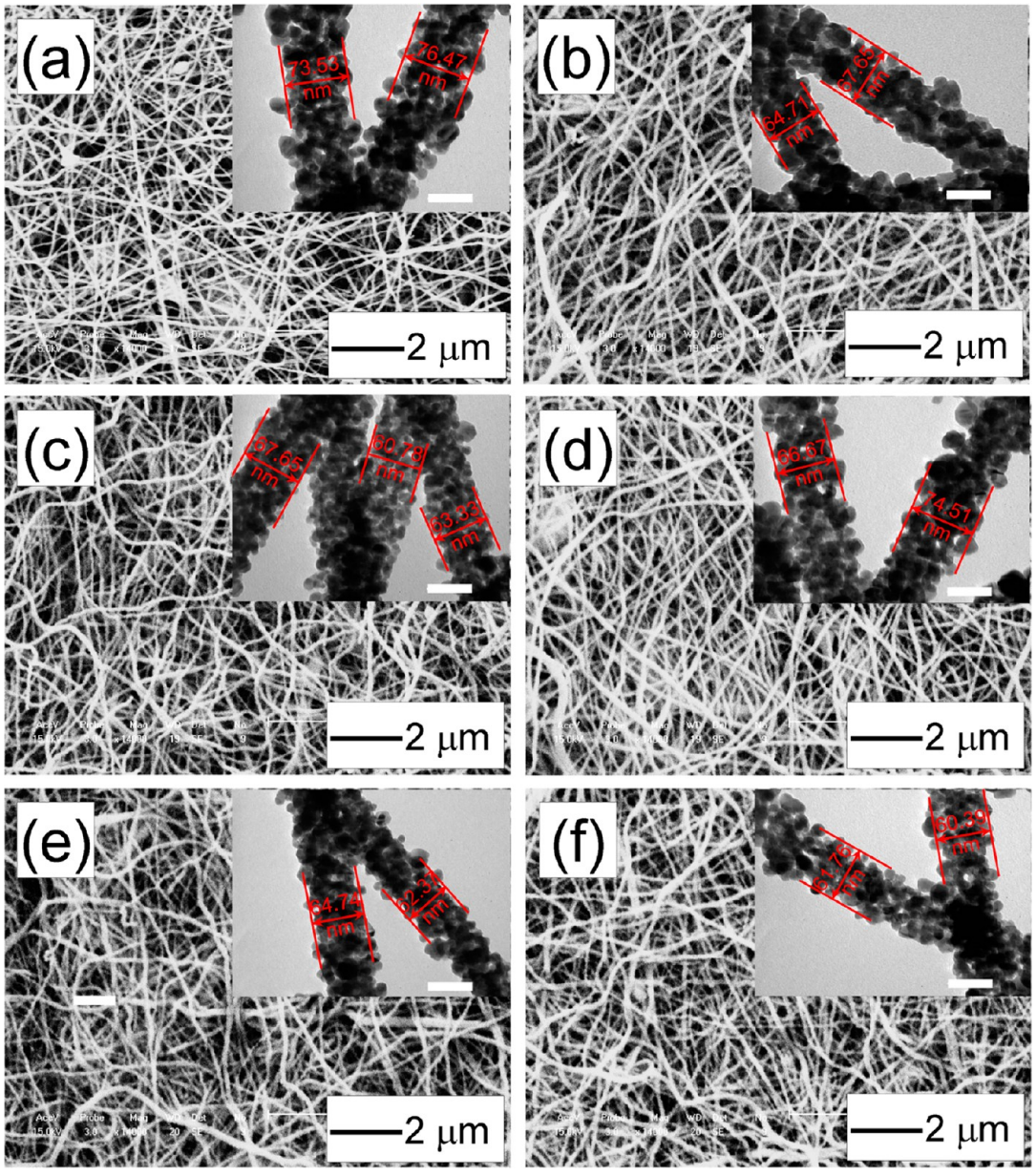

Figure 2. SEM images of (a) unloaded SnO_2 nanofibers, (b) 1, (c) 3, (d) 5, (e) 10, and (f) 30 at % Pd^0-loaded SnO_2 nanofibers. The scale bar is 2 μm. The insets are the magnified TEM images, respectively. The scale bar is 50 nm.

better response to 1000 ppm H_2 compared to the undoped sample.[19] Choi et al. have discussed the tuning of gas selectivity via the combinatorial control of Pd doping concentration in the hollow nanofibers.[20] The molecular adsorbate on the Pd nanocrystals surfaces was dissociated by the enhanced catalytic and diffused to the oxide surface subsequently.[21]

dx.doi.org/10.1021/am3028553 | ACS Appl. Mater. Interfaces 2013, 5, 2013−2021

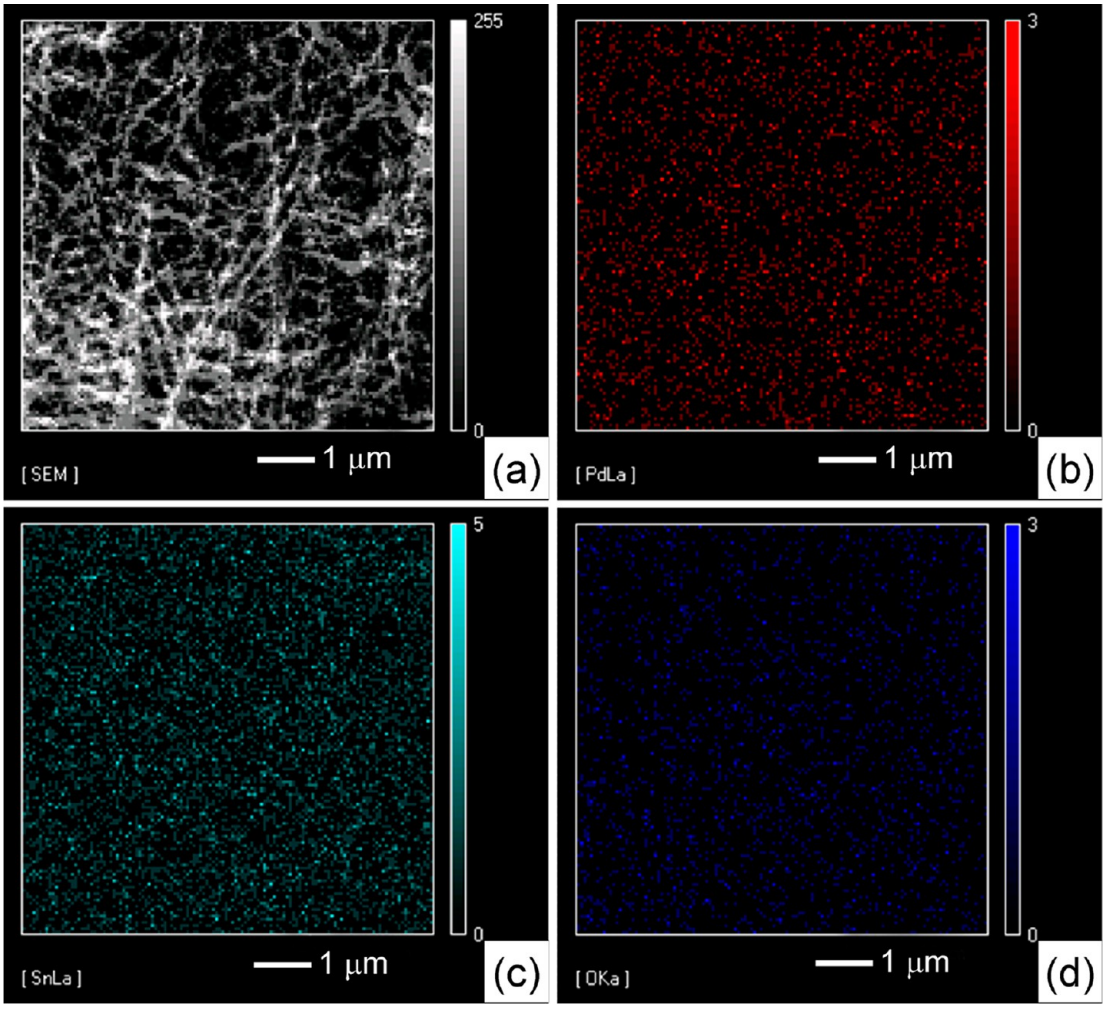

Figure 3. EDX mapping images of the 30 at % Pd^0-loaded SnO_2 nanofibers. (a) The respective SEM images, the distribution of (b) Pd, (c) Sn, and (d) O in the nanofibers.

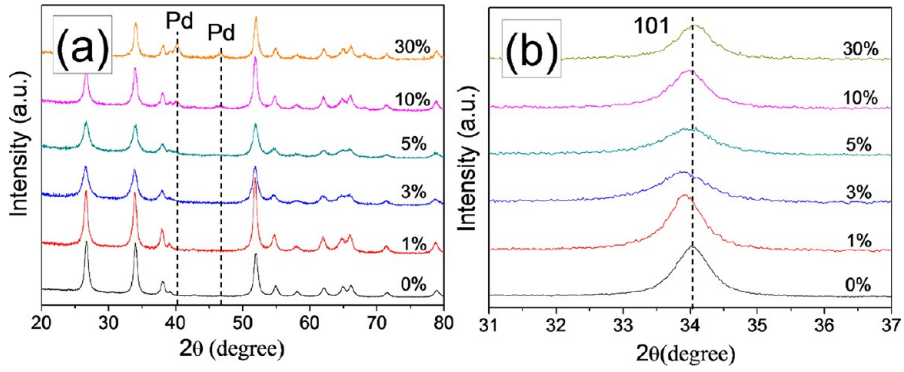

Figure 4. (a) Full-angle range of XRD patterns of pristine and Pd^0-loaded SnO_2 nanofibers. (b) High-resolution of (101) peak.

In our previous work, 1D Pd^{2+}-loaded SnO_2 nanofibers have been successfully prepared combining electrospinning and calcination. Enhanced H_2 sensitivity at lower operating temperature compared with unloaded SnO_2 nanofibers was achieved.[15] Herein, we report the synthesis and H_2 sensing properties of Pd^0-loaded SnO_2 nanofibers. Further improved gas sensing properties such as operating at room temperature and ultralow limit of detection (20 ppb) have been achieved for the Pd^0-loaded SnO_2 nanofibers. The sensing mechanism and the structure−activity relationship of SnO_2 were discussed as well.

2. EXPERIMENTAL SECTION

2.1. Chemicals. Ethanol (>95%), N, N-dimethyl formamide (>95%, DMF) and $SnCl_2{\cdot}2H_2O$ were purchased from Tianjin Chemical Co. (China). $PdCl_2$ and hydrazine hydrate were purchased from Beijing Chemical Co. (China). Poly(vinyl pyrrolidone) (PVP, M_w= 1 300 000) was purchased from Aldrich. All chemicals were used as received without any further purification.

dx.doi.org/10.1021/am3028553 | ACS Appl. Mater. Interfaces 2013, 5, 2013−2021

2.2. Preparation of Pd^0-Loaded SnO_2 Composite Nanofibers. In a typical procedure, 0.4 g of $SnCl_2 \cdot 2H_2O$ was dissolved in 4.4 g of DMF and 4.4 g of ethanol under vigorous stirring for 10 min. Subsequently, 0.8 g of PVP and a suit amount of $PdCl_2$ were added into the above solution under vigorous stirring for 30 min. The mixture was electrospun (voltage: 12 kV; distance between anode and cathode: 20 cm) and followed by sintering at 600 °C for 5 h. The Pd^{2+}-loaded SnO_2 composite nanofibers were immersed into excessive hydrazine hydrate to react for 30 min. The obtained Pd^0-SnO_2 composite nanofibers were washed with deionized water 3 times and then dried in air at 60 °C for night. The pure SnO_2 nanofibers were also obtained with no addition of $PdCl_2$ by the same procedure.

2.3. Fabrication and Measurement of H_2 Gas Sensor Based on Our Products. The as-prepared nanofibers were mixed with deionized water in a weight ratio of 100:25 to form a paste. Fix a pin cross the ceramic tube core to set up the ceramic tube for coating. We then coated the paste with a paint pen on the surface of the ceramic tube which has a pair of gold electrodes printed previously. The coating was required to be uniform and covered gold electrodes completely. The ceramic tube coated with materials dried in the shade and then a Ni−Cr heating wire was inserted in the tube to form a side-heated gas sensor. Panels a and b in Figure 1 shows a schematic image of the as-fabricated sensor and a photograph of the sensor on the socket, respectively.

Gas sensing properties were measured using the CGS-1 intelligent test system (Beijing Elite Tech Co. Ltd., China). When the resistances of all the sensors were stable, saturated target gas was injected into the test chamber (20 L in volume) by a microsyringe through a rubber plug. The saturated target gas was mixed with air (relative humidity was about 25% and room temperature was about 25 °C) by two fans in the analysis system. After the sensor resistances reached a new constant value, the test chamber was opened to recover the sensors in air. All the measurements were performed in a laboratory fume hood. The sensor resistance and response values were acquired by the analysis system automatically. The electrical properties of the sensor were measured by Figure 1c gives out the theoretic diagram of the test circuit. The sensor response was measured between room temperature (RT) and 340 °C. The sensor response is defined as the ratio Ra/Rg, where Ra is the resistance in dry air, and Rg is the resistance in test gas. The response and recovery time tests were carried out by combining gas cylinder (e.g., 1 L jar) and extension cord. A certain concentration of aimed gas was allocated in the gas cylinder. One side of the extension cord connected with a gas sensor and the other side was connected with the bottom case of test chamber. The response and recovery behavior measurement was based on the "insert" and "take out" of the gas cylinder. Here the time taken by the sensor to achieve 90% of the total resistance change was defined as the response time in the case of adsorption or the recovery time in the case of desorption.

Table 1. Calculated Values Based on (101) Crystal Planes for the Unloaded and Pd^0-Loaded SnO_2 Nanofibers

Pd^0-loaded SnO_2 nanofibers (at %)	fwhm (deg)	2θ (deg)	crystalline size (nm)
0	0.62232	34.02	13.2
1	0.67424	33.91922	12.2
3	0.82384	33.87365	10.0
5	0.77457	33.96851	10.6
10	0.72929	33.98009	11.3
30	0.68829	34.05042	11.9

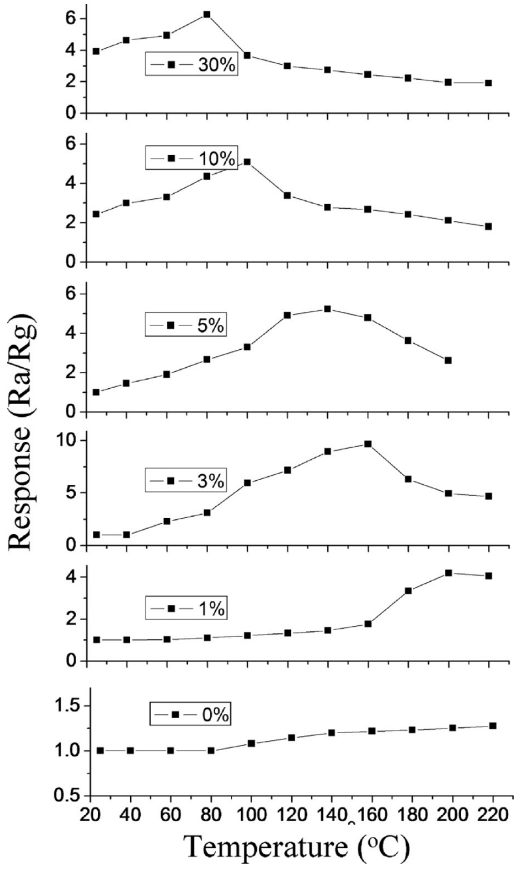

Figure 6. Responses of unloaded and Pd^0-loaded SnO_2 nanofibers with different loading levels against 50 ppm H_2 as a function of operating temperatures.

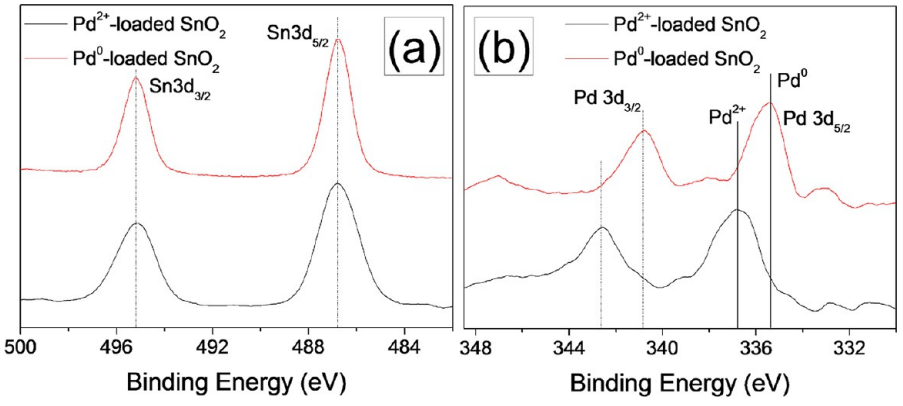

Figure 5. XPS spectra of the (a) Sn 3d and (b) Pd 3d electron binding energies with 30 at % loading level before (black line) and after (red line) in situ reduction.

dx.doi.org/10.1021/am3028553 | ACS Appl. Mater. Interfaces 2013, 5, 2013−2021

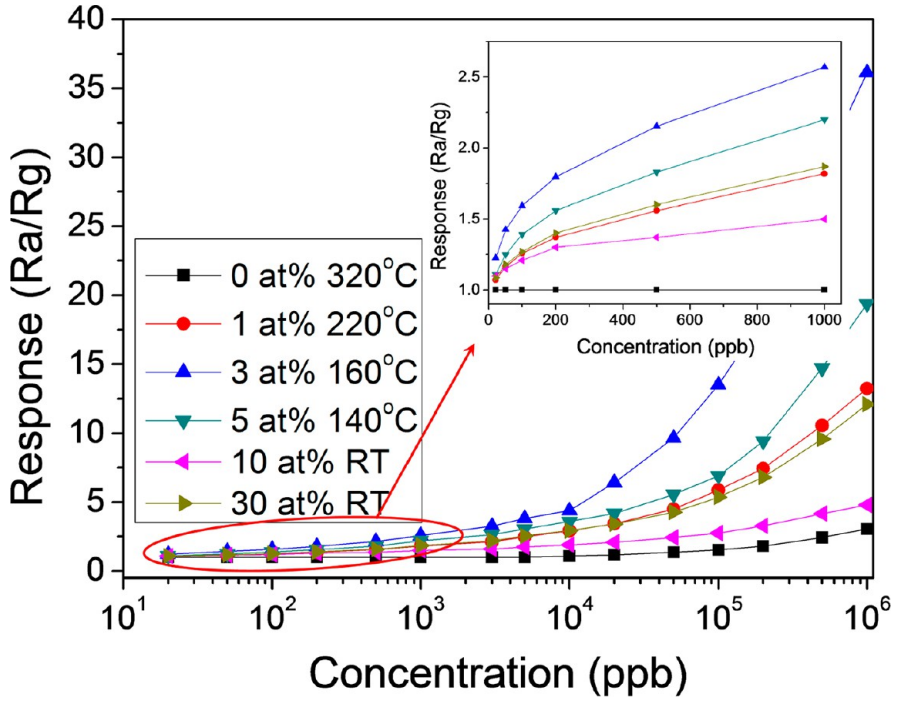

Figure 7. Linear plots of the response of the sensors based on Pd^0-loaded SnO_2 nanofiber against H_2 in the range of 20 ppb to 1000 ppm at different operating temperatures. The inset presents the acceptable response of them at low H_2 concentration.

2.4. Characterization. Nanofibers were characterized by means of scanning electron microscope (SEM, SSX-550, Shimadzu equipped with energy dispersive X-ray (EDX) spectroscopy), transmission electron micrographs (TEM, Hitachi S-570), X-ray diffraction (XRD, PANalytical B.V. Empyrean, standard reflection mode with a Cu Kα source). Analysis of the X-ray photoelectron spectra (XPS) was performed on an ESCLAB MKII using Al as the exciting source.

3. RESULTS AND DISCUSSION

The morphologies characterized by SEM and TEM of SnO_2 nanofibers loaded with different levels of Pd^0 sintered at 600 °C following in situ reduction. As shown in Figure 2, all specimens display the similar disordered and bended fibrous morphology with average diameters ~70 nm. Both large voids between the adjacent fibers and small pores within the final fibers provide easy pathways for gas molecules to penetrate easily into the whole membranes. According to the magnified TEM micrographs, there are slightly changes in nanoparticles diameters.

To characterize the distribution of Pd, we characterized the 30 at % Pd^0-loaded SnO_2 nanofiber nonwoven membrane by EDX of SEM. The elemental-mapping analysis, as shown in Figure 3, revealed that the Pd (red) atoms were homogeneously distributed throughout the Pd^0-loaded SnO_2 composite nanofibers, which were similar to Sn (green) and O (blue) atoms in the composite nanofibers. Pd atoms can distribute homogeneously via our method, which will increase the effective amount of that during reacting with aimed gases.

The crystallization of the electrospun nanofibers as a function of Pd content was examined by X-ray diffraction (XRD). Figure 4a shows the XRD patterns of unloaded and 1, 3, 5, 10, and 30 at % Pd^0-loaded SnO_2 specimens calcined at 600 °C and following in situ reduction in hydrazine hydrate. All of them display clear reflections from the (110), (101), (200), (211), and (220) etc. crystallographic planes of the cassiterite SnO_2 crystalline phase (rutile structure, JCPDS 41−1445, space group $P4_2/mnm$).[22] There is no indication of the presence of any dopant-related diffraction peaks for the Pd^0-loaded level less than 5 at % samples, implying the high dispersion or the poor crystallinity of dopants related nanoparticles. While as for the 10 and 30 at % Pd^0-loaded SnO_2 nanofibers, the peaks at 2θ = 40.2 and 46.8° correspond to the reflection of the cubic structure of Pd^0 (JCPDS File 46−1043).[23] However, two tiny differences between the unloaded and Pd^0-loaded samples can be discerned. One is that the full widths at half-maximum (fwhm) of the diffraction peaks for the loaded samples are slightly larger than that of the unloaded sample, as shown in the enlarged partial view of the XRD patterns (Figure 4b). The crystallite sizes of samples can be estimated by using the Scherrer equation

$$D = \frac{0.9\lambda}{B\cos\theta}$$

Where D is the crystallite size, B is the fwhm, θ is diffraction angle, and λ is the wavelength of X-ray.[24] The estimated crystallite sizes corresponding to (101) crystallographic planes were illustrated in Table 1. In contrast to the pristine SnO_2 nanofibers, the grain sizes within all Pd^0 loaded SnO_2 nanofibers reduced. Another difference lies in the tiny change in the positions of the diffraction peaks in the patterns. Taking the (101) crystallographic planes as an example, the position of the diffraction peaks from Pd^0-loaded SnO_2 specimens shift to lower angles compared to the unloaded SnO_2 specimen at first, confirming the Pd^{2+} is incorporated into the SnO_2 lattice and occupying the tetragonal Sn^{4+} cation sites after calcination (when the concentration of Pd is less or equal to 3 at %). As the concentration of Pd is higher or equal to 5 at %, the (101) peak recovers toward the original degree again, implying that some Pd^{2+} ions cannot be contained within the SnO_2 crystal and expelled from the crystal during the calcination for the different ions radius of Pd^{2+} (86 pm) and Sn^{4+} (69 pm).

The chemical composition of the specimens after calcination and in situ reduction was examined by X-ray photoelectron

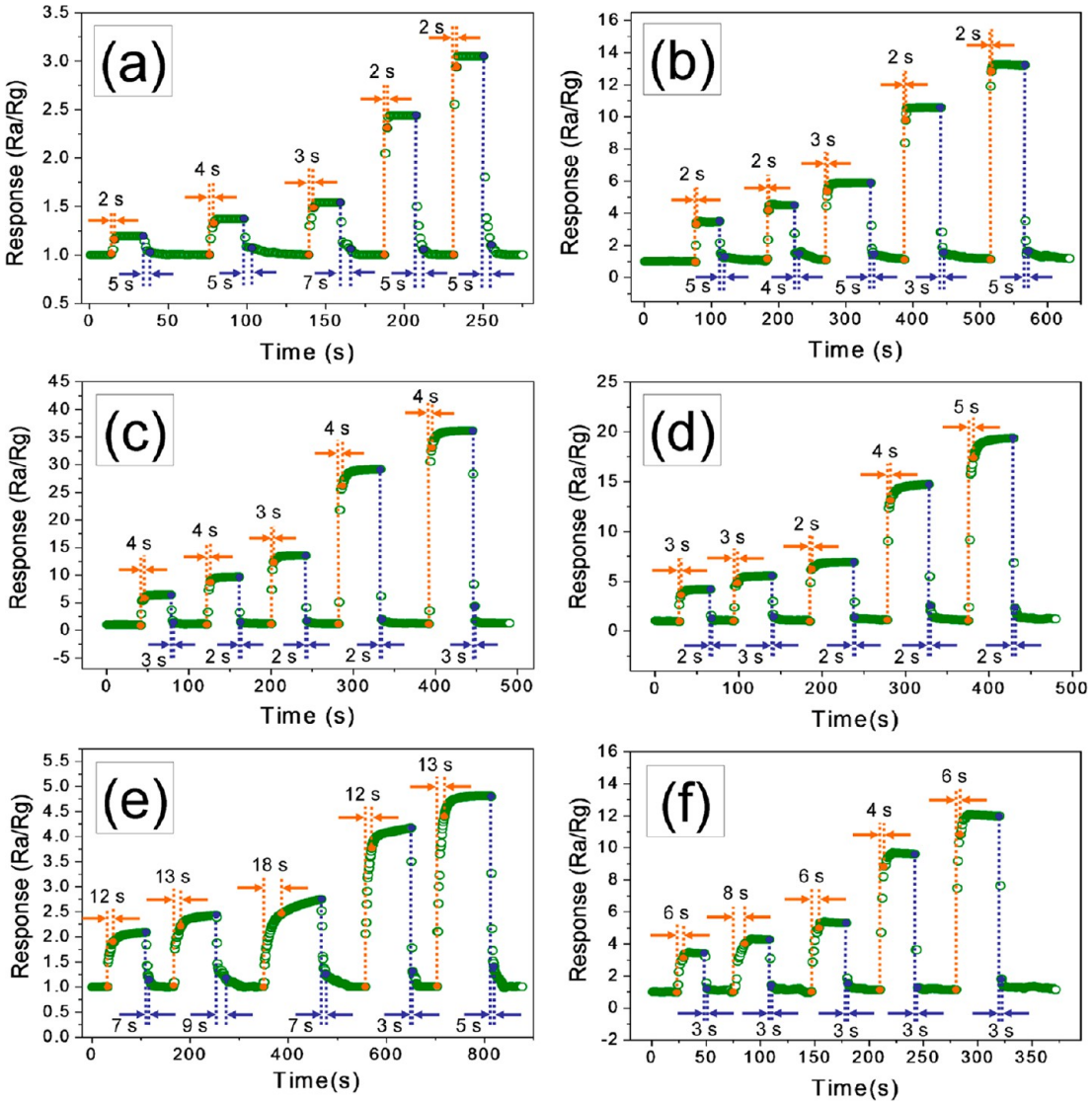

Figure 8. Dynamic H_2 sensing transients of all sensors with different loading levels (a) 0, (b) 1, (c) 3, (d) 5, (e) 10, and (f) 30 at % to 20, 50, 100, 500, and 1000 ppm in turn.

spectroscopy (XPS). Figure 5 shows the Sn 3d and Pd 3d photoemission spectra of 30 at % Pd^0-loaded SnO_2 specimen before and after in situ reduction. The Sn 3d doublet characterized by $3d_{3/2}-3d_{5/2}$ splitting was clearly observed in Figure 5a. In situ reduction in hydrazine hydrate does not produce any significant reduction of Sn^{4+} as detected by XPS. Significant changes, especially the shape of Pd 3d signal, are observed in these spectra. The gap between the Pd $3d_{5/2}$ and Pd $3d_{3/2}$ level is 5.3 eV, which is very close to the spin−orbit doublet separation value reported in the literature.[25] The characteristic peak of Pd $3d_{5/2}$ with binding energy of 336.9 eV corresponds to Pd^{2+} (PdO), and after in situ reduction, the peak shifts to the binding energy of 335.7 eV, which is identified as Pd^0 peak. This indicates that the $PdCl_2$ (338.6) in precursor nanofibers was turned into PdO in SnO_2 nanofibers during the calcinations at 600 °C and finally turned into Pd^0 after in situ reduction.

To examine the gas sensing properties of our electrospun SnO_2 nanofibers and the effect of Pd^0-loading on their sensing properties we fabricated gas sensors comprising different Pd^0-loading levels and measured their resistance response. The optimum working temperature range is an important functional characteristic for semiconducting oxide sensors. Figure 6 shows the response of the sensors to 50 ppm of H_2 at operating temperatures from RT to 220 °C. It can be observed that the sensor based on pure SnO_2 shows no response to 50 ppm H_2 until the operating temperature in the range to 120 °C. And in our previous research the pure SnO_2 nanofibers would exhibit the maximum response of 1.4 at 320 °C. For Pd^0 doped SnO_2 nanofibers, the optimum operating temperatures have significant decreased by increasing the Pd-loaded level, which in turn directly verifies the promotion effect of Pd loading. Satisfyingly, 10 and 30 at % Pd^0-loaded specimens have considerable response at room temperature although their optimized operating temperatures are still much higher than RT (It is important to note that the following systematic analysis was based on their optimum operation temperatures except for the two operating at RT).

Figure 7 shows the response changes based on our specimens with different Pd^0-loaded levels, against different concentrations of H_2 (20−1000 ppm). The largest response is obtained with the 3 at % dopant to the other specimens, in which even at

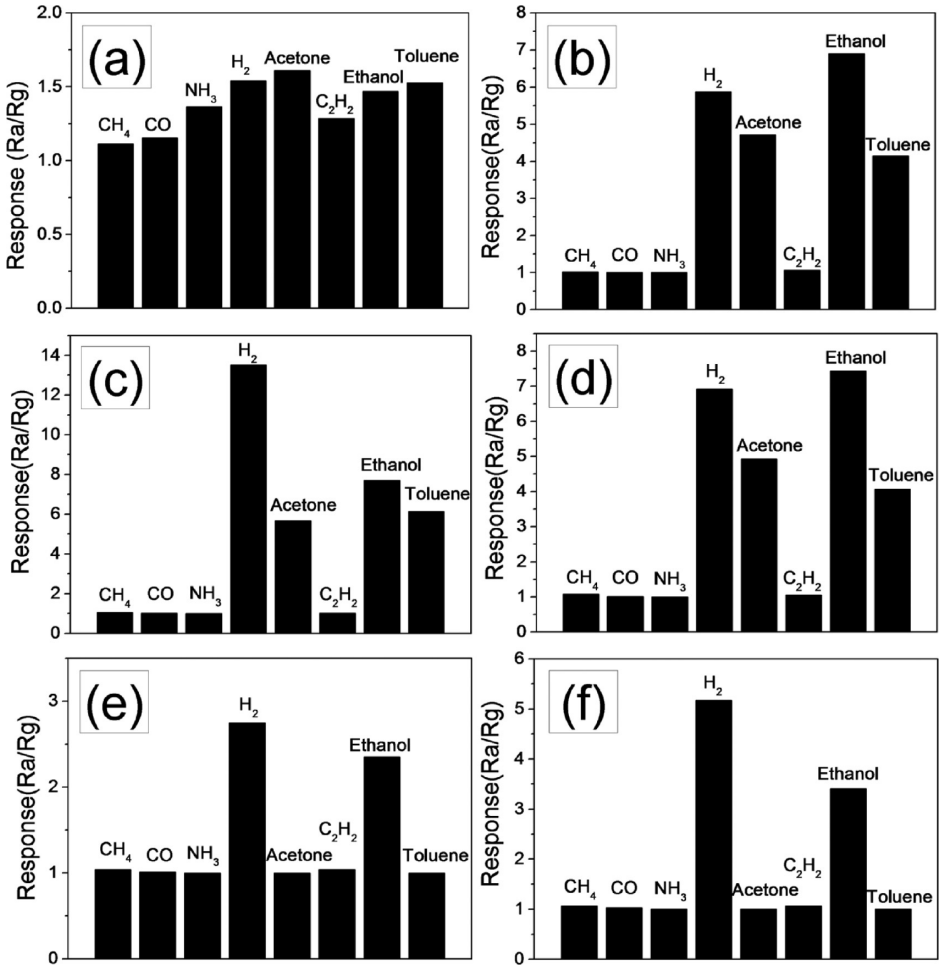

Figure 9. Response of all sensors with different loading levels (a) 0, (b) 1, (c) 3, (d) 5, (e) 10, and (f) 30 at % to 100 ppm different gases at respective operating temperature.

20 ppb of H_2 detectable response can be observed, surpassing most the existed H_2 devices based on SnO_2 nanohybid-structures. The response of our samples increases rapidly with increasing H_2 concentration and still unsaturated at 1000 ppm H_2, confirming a very wide detection scope. The inset in Figure 7 presents the acceptable response of our samples at low H_2 concentration.

The dynamic H_2 sensing transients of all sensors at different operating temperatures are shown in Figure 8. A few cycles were successively recorded, corresponding to different H_2 concentrations ranging from 20 to 1000 ppm. It has been found to be highly dependent on the catalyzer loading. When the Pd^0-loaded level is low (≤5 at %, Figure 8a−d), which were operated at high temperature, they usually have short response (2−5 s) and corresponding recovery (2−7 s) time. As for the sensors operated at RT, their response time is a little longer than the other sensors operated with heating. In contrast, under the same conditions, the 30 at % Pd^0-loaded sample has a much faster response rate than that of 10 at % and a shorter recovery time of only ∼3 s. All of these results are ideal in actual application.

The good selectivity to detect a target gas in the presence of multigas molecules, especially with similar physicochemical properties, is very important toward good sensing element in real-time gas sensing devices. For systematic analysis, the sensitivity values to various gases (CH_4, CO, NH_3, acetone, C_2H_2, ethanol, and toluene) at 100 ppm were measured and the results are presented in Figure 9. Clearly, at high operation temperatures of low Pd^0-loaded specimens, the three species of acetone, ethanol, and toluene are the most interferential gases to H_2. Although the two sensors operated at RT exhibit better selectivity, which almost only response to H_2 and ethanol (the response value of H_2 lies higher than ethanol). The Pd^0 sensitization of SnO_2 nanofibers results in a low operating temperature and a high response to H_2, which is proven to be one of the most effective methods for improving the sensing performance and is potentially useful for the decrease of the power consumption.

To clarify the advantages of the Pd^0-loaded SnO_2 nanofibers in the sensor response to hydrogen, we quantitatively compare our studies with previous works using SnO_2 and other metal oxide electrodes for hydrogen sensing. The comparison of sensor response at different hydrogen concentrations and of various SnO_2 electrodes for hydrogen sensing is summarized in Table 2. To give convictive comparative data, we have made a suitable transformation to these data by $S = R_a/R_g$. Accordingly, these results definitely show that the Pd^0-loaded SnO_2 nanofiber gas sensors have achieved better sensing results than that of SnO_2 electrodes for hydrogen sensing.

The enhanced gas sensing performance can be explained by the following aspects. The first is that the changes on SnO_2 crystal structures. For Pd^0-loaded SnO_2 composite nanofibers, as the Pd (≤3 at %) occupy the tetragonal Sn^{4+} cation sites within the rutile, large crystal lattice distortion will generate,

dx.doi.org/10.1021/am3028553 | ACS Appl. Mater. Interfaces 2013, 5, 2013−2021

Table 2. Brief Summary of Results Reported on SnO_2-Based H_2 Sensors[a]

	concentration						
	20 ppb	1 ppm	10 ppm	500 ppm	1000 ppm	3%	
materials	R_a/R_g						T (°C)
SnO_2 film[26,27]			1.18				300
SnO_2 nanorod[28]				1.4			300
SnO_2 nanowire[28]					4.25		300
SnO_2 nanobelt[29]						1.6	80
SnO_2 nanofiber		1	1.09	2.44	3.05		320
3% Pd^{2+}-doped SnO_2 nanofiber[15]				16	26.5		280
30% Pd^{2+}-loaded SnO_2 nanofiber[30]		~3					350
3% Pd^0-loaded SnO_2 nanofiber	1.22	2.57	4.39	29.14	36.14		160
30% Pd^0-loaded SnO_2 nanofiber	1.09	1.87	2.93	9.59	12.09		RT

[a]All the values were read from the corresponding references and converted as Ra/Rg for comparison.

causing the increasement of oxygen vacancy in the final product. Additionally, such large crystal lattice distortion will further prevent the growth of SnO_2 crystal and lower the gain size of SnO_2 crystal within the final product as well. As the concentration of Pd is higher or equal to 5 at %, some Pd^{2+} ions can not be contained within the SnO_2 crystal and expelled from the crystal during the calcination. After in situ reduction, Pd^0 was loaded on the surface of SnO_2 nanocrystals. In this case, the observed magnitude of the changes in sensing properties, kinetics and temperature dependence brought about by Pd^0 functionalization can be explained by "electronic mechanism" and "chemical mechanism". In the electronic mechanism, the sensitization is promoted by direct exchange of electrons between the semiconductor and the metal additive nanocrystals.[31] When gas molecules are chemisorbed on the Pd^0 nanocrystals, their electronic density or even their oxidation state may change, the work function of Pd^0 nanocrystals being also affected. These facts modify the electron exchange properties between the metal nanocrystals and the semiconductor substrate, and consequently, the electronic conductivity in the SnO_2 is modified.[32−36] On the other hand, it proposes that the Pd nanocrystals catalytically activate the dissociation of molecular oxygen on the surface of metal oxide substrates, resulting in the increase in length of the depleted layer together with the width and height of potential barrier. When the samples were exposed upon reducing gas, the depleted layer was fading away, thus the width and height of the barrier potential decreased, leading to the decrease in sensor resistance.[37]

4. CONCLUSIONS

In summary, a simple route was successfully promoted to synthesize novel Pd^0-loaded SnO_2 nanofibers. The as-prepared SnO_2 sample consists of different Pd^0-loaded levels have been investigated as hydrogen sensors in detail. By adjusting the Pd^0-loaded levels, high sensing performance such as high response, low detection limit (20 ppb), fast response (4−13 s) and recovery (3−9 s), and high selectivity toward H_2 can be obtained at room temperature. The excellent sensing performances are attributed to the changes in crystalline structure and catalytic effect of Pd^0.

AUTHOR INFORMATION

Corresponding Author

*E-mail: askyu224901@yahoo.com.cn (Z.L.); cwang@jlu.edu.cn (C.W.). Tel.: +86 431 85168292. Fax: +86 431 85168292.

Notes

The authors declare no competing financial interest.

ACKNOWLEDGMENTS

The work has been supported by National 973 Project (2007CB936203 and S2009061009), NSF China (51003036), Jilin Province Key Project (20110339), and Doctoral Interdisciplinary Sponsored Research Project of Jilin University (2012JC006).

REFERENCES

(1) Dresselhaus, M. S.; Thomas, I. L. *Nature* **2001**, *414*, 332−337.
(2) Iwanaga, T.; Hyodo, T.; Shimizu, Y.; Egashira, M. *Sens. Actuators, B.* **2003**, *93*, 519−525.
(3) Sumida, S.; Okazaki, S.; Asakura, S.; Nakagawa, H.; Murayama, H.; Hasegawa, T. *Sens. Actuators, B* **2005**, *108*, 508−514.
(4) Yamazaki, T.; Okumura, H.; Jin, C. J.; Nakayama, A.; Kikuta, T.; Nakatani, N. *Vaccum* **2005**, *77*, 237−243.
(5) Mishra, V. N.; Agarwal, R. P. *Microelectron. J.* **1998**, *29*, 861−874.
(6) Dolbec, R.; El-Khakani, M. A.; Serventi, A. M.; Saint-Jacques, R. G. *Sens. Actuators, B* **2003**, *93*, 566−571.
(7) Baik, N. S.; Sakai, G.; Miura, N.; Yamazoe, N. *Sens. Actuators, B* **2000**, *63*, 74−79.
(8) Shimizu, Y.; Kai, S.; Takao, Y.; Hyodo, T.; Egashira, M. *Sens. Actuators, B* **2000**, *65*, 349−357.
(9) Kawahara, A.; Yoshihara, K.; Katsuki, H.; Shimizu, Y.; Egashira, M. *Sens. Actuators, B* **2000**, *65*, 17−22.
(10) Wada, K.; Egashira, M. *Sens. Actuators, B* **2000**, *62*, 211−219.
(11) Ponzoni, A.; Comini, E.; Sberveglieri, G. *Appl. Phys. Lett.* **2006**, *88* (203101), 3.
(12) Huang, H.; Ong, C. Y.; Guo, J.; White, T.; Tse, M. S.; Tan, O. K. *Nanoscale* **2010**, *2*, 1203−1207.
(13) Wang, Z. J.; Li, Z. Y.; Sun, J. H.; Zhang, H. N.; Wang, W.; Zheng, W.; Wang, C. *J. Phys. Chem. C* **2010**, *114*, 6100−6105.
(14) Xu, X. R.; Sun, J. H.; Zhang, H. N.; Wang, Z. J.; Dong, B.; Jiang, T. T.; Wang, W.; Li, Z. Y.; Wang, C. *Sens. Actuators, B* **2011**, *160*, 858−863.
(15) Zhang, H. N.; Li, Z. Y.; Liu, L.; Xu, X. R.; Wang, Z. J.; Wang, W.; Zheng, W.; Dong, B.; Wang, C. *Sens. Actuators, B* **2010**, *147*, 111−115.
(16) Liu, L.; Guo, C. C.; Li, S. C.; Wang, L. Y.; Dong, Q. Y. *Sens. Actuators, B* **2010**, *150*, 806−810.
(17) Lewis, F. A. *Platinum Met. Rev.* **1982**, *26*, 20−27.
(18) Flanagan, T. B.; Oates, W. A. *Annu. Rev. Mater. Sci.* **1991**, *21*, 269−304.
(19) Lee, Y. C.; Huang, Hui; Tan, O. K.; Tse, M. S. *Sens. Actuators, B* **2008**, *132*, 239−242.
(20) Choi, J. K.; Hwang, I. S.; Kim, S. J.; Park, J. S.; Park, S. S.; Jeong, U.; Kang, Y. C.; Lee, J. H. *Sens. Actuators, B: Chem.* **2010**, *150*, 191−199.

(21) Kolmakov, A.; Klenov, D. O.; Lilach, Y.; Stemmer, S.; Moskovits, M. *Nano Lett.* **2005**, *5*, 667−673.
(22) Haridas, D.; Gupt, V. *Sens. Actuators, B: Chem.* **2012**, *166−167*, 156−164.
(23) Kim, S. S.; Park, J. Y.; Choi, S. W.; Na, H. G.; Yang, J. C.; Kim, H. W. *J. Alloys Compd.* **2011**, *509*, 9171−9177.
(24) Patterson, A. L. *Phys. Rev.* **1939**, *56*, 978−982.
(25) Jiménez, V. M.; Espinós, J. P.; González-Elipe, A. R. *Sens. Actuators, B* **1999**, *61*, 23−32.
(26) Wheeler, M. C.; Tiffany, J. E.; Walton, R. M.; Cavicchi, R. E.; Semancik, S. *Sens. Actuators, B* **2001**, *77*, 167−176.
(27) Cavicchi, R. E.; Suehle, J. S.; Kreider, K. G.; Shomaker, B. L.; Small, J. A.; Gaitan, M.; Chaparala, P. *Appl. Phys. Lett.* **1995**, *66* (812), 3.
(28) Wang, B.; Zhu, L. F.; Yang, Y. H.; Xu, N. S. *J. Phys. Chem. C* **2008**, *112*, 6643−6647.
(29) Kind, L. H.; Messer, B.; Kim, F.; Yang, P. *Angew. Chem., Int. Ed.* **2002**, *41*, 2405−2408.
(30) Yang, D. J.; Kamienchick, I.; Youn, D. Y.; Rothschild, A.; Kim, I. D. *Adv. Funct. Mater.* **2010**, *20*, 4258−4264.
(31) Zhdanov, V. P. *Surf. Sci.* **2002**, *512*, L331−L334.
(32) Kim, J. C.; Jun, H. K.; Huh, J. S.; Lee, D. D. *Sens. Actuators, B* **1997**, *45*, 271−277.
(33) Papadopoulos, C. A.; Vlachos, D. S.; Avaritsiotis, J. N. *Sens. Actuators, B* **1996**, *32*, 61−69.
(34) Angelis, L.; Riva, R. *Sens. Actuators, B: Chem.* **1995**, *28*, 25−29.
(35) Ivanovskava, M. I.; Bogdanov, P. A.; Orlik, D. R.; Gurlo, A. C.; Romanovkaya, V. V. *Thin Solid Films* **1997**, *296*, 41−43.
(36) Xing, L. L.; Ma, C. H.; Chen, Z. H.; Chen, Y. J.; Xue, X. Y. *Nanotechnology* **2011**, *22* (215501), 7.
(37) Liu, H.; Gong, S. P.; Hu, Y. X.; Liu, J. Q.; Zhou, D. X. *Sens. Actuators, B* **2009**, *140*, 190−195.